

# Impact of the orbital current order on the superconducting properties of the kagome superconductors

Hong-Min Jiang,<sup>1,\*</sup> Ming-Xun Liu,<sup>1</sup> and Shun-Li Yu<sup>2,†</sup>

<sup>1</sup>*School of Science, Zhejiang University of Science and Technology, Hangzhou 310023, China*

<sup>2</sup>*School of Physics, National Laboratory of Solid State Microstructures, Nanjing University, Nanjing 210093, China*

(Dated: February 27, 2023)

Motivated by recent experimental evidences signalling the chiral charge order in the vanadium-based kagome superconductors, we theoretically investigate the impact of the chiral flux charge order over the experimental outcomes for the normal and the SC properties. It is revealed that the spectral weight on the Fermi surface (FS) is partially gaped by the chiral flux charge order with the reservation of the spectral weight on the  $M$  points and the midpoint between the two adjacent  $M$  points, resulting in the momentum-dependent energy gap being consistent with the recent experimental observations. More importantly, by considering the influence of the chiral flux charge order, we find that a conventional fully gapped SC pairing state evolves into a nodal gap feature for the spectral weight due to the spectral gap modulations on the FS. As a result, the U-shaped density of states (DOS) deforms to the V-shaped one along with the residual DOS near the Fermi energy. These results bear some resemblance to the experimental observations, and may serve as a promising proposal to mediate the divergent or seemingly contradictory experimental outcomes about the SC pairing symmetry.

PACS numbers: 74.20.Mn, 74.25.Ha, 74.62.En, 74.25.nj

## I. INTRODUCTION

The recent discovery of superconductivity in a family of compounds  $AV_3Sb_5$  ( $A=K, Rb, Cs$ ), which share a common lattice structure with kagome net of vanadium atoms, has triggered a new surge of interest in the investigation of superconductivity<sup>1–37</sup>. The fascinating aspects of these materials lie in the exotic quantum physics as they integrate with the geometrical lattice frustration, the van Hove filling, the nontrivial band topology, and the interplay between the charge density wave and superconductivity<sup>12,38–41</sup>, which makes the emergence of superconductivity in these materials is in themselves exotic and rare.

A central issue about the superconductivity is to unveil the superconducting (SC) pairing mechanism. To search for clues to this puzzling question, the determination of the pairing symmetry of the SC order parameter is thought to be a prerequisite step. However, the inconsistent or even contradicting results have been found so far in experimental measurements and data analyses. The temperature dependence of the nuclear spin-lattice relaxation rate shows a Hebel-Slichter coherence peak just below  $T_c$ , indicating that  $CsV_3Sb_5$  is a conventional  $s$ -wave superconductor<sup>15</sup>. The penetration depth measurements also lend support to such a view<sup>16</sup>. Nevertheless, the measurements of thermal conductivity on  $CsV_3Sb_5$  at ultra-low temperature evidenced a finite residual linear term, pointing to an unconventional nodal SC gap<sup>17</sup>. In accordance with this, the V-shaped SC gaps with residual zero-energy density of states (DOS) also suggest an anisotropic SC gap with nodes<sup>12–14</sup>. Moreover, the scanning tunnelling microscope/spectroscopy (STM/STS) experiment on  $CsV_3Sb_5$  at ultra-low temperature revealed a two-gap structure with multiple sets

of coherent peaks and residual zero-energy DOS, accompanied by the magnetic/non-magnetic impurity effects, implying a rather novel and interesting SC gap, i.e., the sign preserved multiband superconductivity with gap nodes<sup>13</sup>.

Theoretically, the results about the pairing symmetries vary widely as well, depending on the different methods and models. Early before the discovery of the superconductivity in  $AV_3Sb_5$ , while a chiral  $d_{x^2-y^2} + id_{xy}$ -wave SC state was predicted to be the most favorable one within a reasonable parameter range for the van Hove filling kagome system based on the variational cluster approach and the perturbative renormalization group analysis to a single-orbital Hubbard model<sup>38,39</sup>, the singular-mode functional renormalization group theory discovered a rich variety of electronic instabilities ranging from  $s$ -wave and  $d$ -wave to  $d_{x^2-y^2} + id_{xy}$ -wave superconductivities under short-range interactions<sup>40</sup>. Later on, with the inspiration from the discovery of superconductivity in the family of  $AV_3Sb_5$ , a random phase approximation based on a two-orbital model revealed an  $f$ -wave pairing instability over a large range of coupling strength, succeeded by  $d$ -wave singlet pairing for stronger coupling<sup>42</sup>. On the other hand, the determinant quantum Monte Carlo calculations on the kagome-lattice Hubbard model found the dominating pairing channel was  $d_{x^2-y^2} + id_{xy}$  ( $s_{ex}$ )-wave in the hole (electron)-doped case<sup>43</sup>. What is more, it has been uncovered that the mechanism of bond-order fluctuations could give rise to both singlet  $s$ -wave and triplet  $p$ -wave superconductivity<sup>44</sup>. Nevertheless, the experimental controversy concerning the SC pairing symmetry in the family of  $AV_3Sb_5$  remains unsettled.

One of the reasons for the divergent experimental outcomes lies in that the SC order may intertwine with other unconventional electron orders, adding another layer of

complexity to this already challenging issue in the field. Although the possibility of long-range magnetic order in the  $\text{AV}_3\text{Sb}_5$  crystal has been ruled out by the neutron scattering<sup>45</sup> and muon spin spectroscopy<sup>46</sup> measurements, a giant anomalous Hall effect has still been observed above the entrance of the SC state with the concomitant onset of a  $2 \times 2$  charge density wave (CDW) order<sup>2,9</sup>, indicating this time-reversal symmetry-breaking transition derives primarily from the charge degree of freedom<sup>46</sup>. So far, there are an increasing number of experimental evidences supporting that the CDW state has a  $2 \times 2$  chiral flux order<sup>8,27,37,47–53</sup>. Furthermore, the muon spin relaxation technic observed a noticeable enhancement of the internal field width, which takes place just below the charge ordering temperature and persists into the SC state<sup>47</sup>, pointing to time-reversal symmetry-breaking charge order intertwining with unconventional superconductivity. Thus, the chiral CDW should be considered in analyzing the SC properties in the vanadium-based kagome superconductors.

Given the fairly good Fermi surface (FS) nesting and proximity to the von Hove singularity, the system is prone to the instability of “triple- $Q$ ” CDW at the three nesting wave vectors<sup>54–62</sup>. While the real component of the “triple- $Q$ ” bond charge order conforms to the modulated superlattice pattern uncovered in the experiments, the theoretical proposal of “triple- $Q$ ” imaginary CDWs, which was originally put forward on the honeycomb and triangular lattices<sup>54,55</sup>, appears consistent simultaneously with the superlattice modulations and the time-reversal symmetry breaking. Subsequently, various chiral flux phases with different configurations of orbital current have been proposed in a series of theoretical studies on the kagome superconductors<sup>56–61</sup>. A recent self-consistent mean-field study has shown that the chiral CDW in Fig. 1(a) can be stabilized by moderately small intersite Coulomb interactions and it might be the most relevant time-reversal symmetry-breaking state in  $\text{AV}_3\text{Sb}_5$ <sup>63</sup>. In addition, the coexistence of the chiral CDW with a conventional fully gapped superconductivity could lead to gapless edge modes on the domains of the lattice symmetry breaking order<sup>61</sup>. These edge modes with gapless excitations could account for the residual DOS and the finite residual thermal conductivity. However, there is still lack of a systematic investigation on the direct influence of the chiral CDW over the SC pairing properties, especially when one considers the growing experimental evidences pointing to the persistence of the time-reversal symmetry-breaking CDW well into the SC state<sup>8,37,64</sup>.

In this paper, we aim to fill up the blank by showing that the chiral flux phase in Fig. 1(a) as a representative of the time-reversal symmetry-breaking  $2 \times 2$  CDW has a profound impact on the experimental outcomes with respect to both the normal and the SC properties. By unfolding the spectral weight function and the energy bands to the primitive Brillouin zone (PBZ), we show that only portions of the FS are gaped by the CDW or-

der. While the original band near the saddle point is split into three sub-bands by the CDW order, three new saddle points emerge in the CDW phase, and especially there is still an obvious residual saddle-point spectrum at the Fermi level. Importantly, the novelty we discovered in the calculations is such that a conventional fully gapped SC pairing state will acquire a nodal gap feature for the spectral weight on the FS when the impact of the chiral flux CDW order is taken into account. The nodal gap feature manifests itself as the evolution from the U-shaped DOS to the V-shaped one along with the residual DOS near the Fermi energy, which is the direct outcome of the charge order induced gap modulations of the spectral function on the FS. These results not only account for some experimental observations, but also provide an alternative scenario to reconcile the divergent or seemingly contradictory experimental outcomes regarding the SC pairing symmetry.

The remainder of the paper is organized as follows. In Sec. II, we introduce the model Hamiltonian and carry out analytical calculations. In Sec. III, we present numerical calculations and discuss the results. In Sec. IV, we make a conclusion.

## II. MODEL AND METHOD

The  $2 \times 2$  CDW order quadruply enlarges the unit cell, as indicated by the dashed lines in Fig. 1(a). Among the possible time-reversal symmetry-breaking charge order configurations, the chiral flux phase with configuration of the orbital current shown in Fig. 1(a) has been found to be energetically favorable<sup>59</sup>. Thus, we adopt this typical CDW configuration as a representative of the demonstration, and leave other possibilities for future researches. It is widely believed that the inter-scattering between three van Hove points with wave vectors  $\mathbf{Q}_a = (0, 2\pi/\sqrt{3})$ ,  $\mathbf{Q}_b = (-\pi, -\pi/\sqrt{3})$  and  $\mathbf{Q}_c = (\pi, -\pi/\sqrt{3})$  causes the CDW in  $\text{AV}_3\text{Sb}_5$  [The wave vectors are shown in Fig. 1(b)]. Meanwhile, the van Hove filling was also proposed to be crucial to the superconductivity in  $\text{AV}_3\text{Sb}_5$ . A single orbital tight binding model near the van Hove filling produces the essential feature of the FS and the van Hove physics. Therefore, to capture the main physics of the topological CDW and its impacts on the SC in  $\text{AV}_3\text{Sb}_5$ , we adopt a minimum single orbital model.

The single orbital model involving the effective electron hoppings on a kagome lattice can be described by the following tight-binding Hamiltonian,

$$H_0 = -t \sum_{\langle \mathbf{i}\mathbf{j} \rangle \sigma} (c_{\mathbf{i}\sigma}^\dagger c_{\mathbf{j}\sigma} + h.c.) - \mu \sum_{\mathbf{i}\sigma} c_{\mathbf{i}\sigma}^\dagger c_{\mathbf{i}\sigma}, \quad (1)$$

where  $c_{\mathbf{i}\sigma}^\dagger$  creates an electron with spin  $\sigma$  on the site  $\mathbf{r}_i$  of the kagome lattice and  $\langle \mathbf{i}\mathbf{j} \rangle$  denotes nearest-neighbors (NN).  $t$  is the hopping integral between the NN sites, and  $\mu$  stands for the chemical potential. The Hamiltonian  $H_0$

can be written in the momentum space as,

$$H_0(\mathbf{k}) = \sum_{\mathbf{k}\sigma} \hat{\Psi}_{\mathbf{k}\sigma}^\dagger \hat{\mathcal{H}}_{\mathbf{k}}^0 \hat{\Psi}_{\mathbf{k}\sigma}, \quad (2)$$

with  $\hat{\Psi}_{\mathbf{k}\sigma} = (c_{A\mathbf{k}\sigma}, c_{B\mathbf{k}\sigma}, c_{C\mathbf{k}\sigma})^T$  and

$$\hat{\mathcal{H}}_{\mathbf{k}}^0 = \begin{pmatrix} -\mu & -2t \cos k_1 & -2t \cos k_2 \\ -2t \cos k_1 & -\mu & -2t \cos k_3 \\ -2t \cos k_2 & -2t \cos k_3 & -\mu \end{pmatrix}. \quad (3)$$

The index  $m = A, B, C$  in  $c_{m\mathbf{k}\sigma}$  labels the three basis sites in the triangular primitive unit cell (PUC).  $k_n$  is abbreviated from  $\mathbf{k} \cdot \boldsymbol{\tau}_n$  with  $\tau_1 = \hat{x}/2$ ,  $\tau_2 = (\hat{x} + \sqrt{3}\hat{y})/4$  and  $\tau_3 = \tau_2 - \tau_1$  denoting the three NN vectors. The spectral function of  $H_0(\mathbf{k})$  defined as  $A^0(\mathbf{k}, E) = -\frac{1}{\pi} \text{Tr}[\text{Im}\hat{G}^0(\mathbf{k}, iE \rightarrow E + i0^+)]$  with  $\hat{G}^0(\mathbf{k}, iE) = [iE\hat{I} - \hat{\mathcal{H}}_{\mathbf{k}}^0]^{-1}$ . Near the van Hove filling with  $1/6$  hole doping, the spectral function at zero energy  $E = 0$  produces the hexagonal FS and the van Hove singularities at  $M$  points, as shown in Fig. 1(b), which produce the essences of the FS and energy band observed in the angle-resolved photoemission spectroscopy (ARPES) experiment and the density functional theory calculations<sup>1</sup>.

The second part of the Hamiltonian accounts for the chiral flux CDW order,

$$H_C = i\lambda \sum_{\langle ij \rangle \sigma} \eta_{ij} (c_{i\sigma}^\dagger c_{j\sigma} - h.c.), \quad (4)$$

where  $\lambda$  denotes the strength of the orbital current order, and  $\eta_{ij} = +1$  if the hopping is positioned in the same direction of the orbital current and otherwise  $\eta_{ij} = -1$ .

The third term accounts for the SC pairing. It reads

$$H_P = \sum_{\mathbf{i}} (\Delta c_{\mathbf{i}\uparrow}^\dagger c_{\mathbf{i}\downarrow}^\dagger + h.c.). \quad (5)$$

The on-site  $s$ -wave SC order parameter  $\Delta = -V\langle c_{\mathbf{i}\uparrow} c_{\mathbf{i}\downarrow} \rangle$  is assumed to derive from the effective interaction between electrons. In the calculations, we choose the typical values of the effective pairing interaction  $V = 1.6$ . Varying the pairing interaction will change the pairing amplitude, but the results presented here will be qualitatively unchanged if the CDW order strength changes in parallel.

In the coexistence of SC and chiral flux  $2 \times 2$  CDW orders, the total Hamiltonian  $H = H_0 + H_P + H_C$  can be written in the momentum space within one enlarged unit cell (EUC) shown in Fig. 1(a) as,

$$\begin{aligned} H(\mathbf{k}) = & -t \sum_{\mathbf{k}, \langle \tilde{\mathbf{i}}\tilde{\mathbf{j}} \rangle, \sigma} [c_{\tilde{\mathbf{k}}\tilde{\mathbf{i}}\sigma}^\dagger c_{\tilde{\mathbf{k}}\tilde{\mathbf{j}}\sigma} e^{-i\mathbf{k} \cdot (\mathbf{r}_{\tilde{\mathbf{i}}} - \mathbf{r}_{\tilde{\mathbf{j}}})} + h.c.] \\ & -\mu \sum_{\mathbf{k}, \tilde{\mathbf{i}}, \sigma} c_{\tilde{\mathbf{k}}\tilde{\mathbf{i}}\sigma}^\dagger c_{\tilde{\mathbf{k}}\tilde{\mathbf{i}}\sigma} \\ & + i\lambda \sum_{\mathbf{k}, \langle \tilde{\mathbf{i}}\tilde{\mathbf{j}} \rangle, \sigma} \eta_{\tilde{\mathbf{i}}\tilde{\mathbf{j}}} [c_{\tilde{\mathbf{k}}\tilde{\mathbf{i}}\sigma}^\dagger c_{\tilde{\mathbf{k}}\tilde{\mathbf{j}}\sigma} e^{-i\mathbf{k} \cdot (\mathbf{r}_{\tilde{\mathbf{i}}} - \mathbf{r}_{\tilde{\mathbf{j}}})} - h.c.] \\ & + \sum_{\mathbf{k}, \tilde{\mathbf{i}}} (\Delta c_{\tilde{\mathbf{k}}\tilde{\mathbf{i}}\uparrow}^\dagger c_{-\tilde{\mathbf{k}}\tilde{\mathbf{i}}\downarrow}^\dagger + h.c.), \end{aligned} \quad (6)$$

where  $\tilde{\mathbf{i}} \in \text{EUC}$  represents the lattice site being within one EUC, and  $\langle \tilde{\mathbf{i}}\tilde{\mathbf{j}} \rangle$  denotes the NN sites with the periodic boundary condition implicitly assumed. Accordingly, the summation of  $\mathbf{k}$  should be in principle over the reduced Brillouin zone (RBZ) as enveloped by the white dashed lines in Fig. 1(c).

Based on the Bogoliubov transformation, we obtain the following Bogoliubov-de Gennes equations in the EUC,

$$\sum_{\mathbf{k}} \sum_{\tilde{\mathbf{j}}} \begin{pmatrix} H_{\tilde{\mathbf{i}}\tilde{\mathbf{j}}, \sigma} & \Delta_{\tilde{\mathbf{i}}\tilde{\mathbf{j}}} \\ \Delta_{\tilde{\mathbf{i}}\tilde{\mathbf{j}}}^* & -H_{\tilde{\mathbf{i}}\tilde{\mathbf{j}}, \bar{\sigma}} \end{pmatrix} \exp[i\mathbf{k} \cdot (\mathbf{r}_{\tilde{\mathbf{j}}} - \mathbf{r}_{\tilde{\mathbf{i}}})] \begin{pmatrix} u_{n, \tilde{\mathbf{j}}, \sigma}^{\mathbf{k}} \\ v_{n, \tilde{\mathbf{j}}, \bar{\sigma}}^{\mathbf{k}} \end{pmatrix} = E_n^{\mathbf{k}} \begin{pmatrix} u_{n, \tilde{\mathbf{i}}, \sigma}^{\mathbf{k}} \\ v_{n, \tilde{\mathbf{i}}, \bar{\sigma}}^{\mathbf{k}} \end{pmatrix}, \quad (7)$$

where  $H_{\tilde{\mathbf{i}}\tilde{\mathbf{j}}, \sigma} = (-t + i\lambda\eta_{\tilde{\mathbf{i}}\tilde{\mathbf{j}}})\delta_{\tilde{\mathbf{i}}+\tau_{\tilde{\mathbf{j}}}, \tilde{\mathbf{j}}} - \mu\delta_{\tilde{\mathbf{i}}, \tilde{\mathbf{j}}}$  with  $\tau_{\tilde{\mathbf{j}}}$  denoting the four NN vectors and  $\Delta_{\tilde{\mathbf{i}}\tilde{\mathbf{j}}} = \Delta\delta_{\tilde{\mathbf{i}}, \tilde{\mathbf{j}}}$ .  $u_{n, \tilde{\mathbf{i}}, \sigma}^{\mathbf{k}}$  and  $v_{n, \tilde{\mathbf{i}}, \bar{\sigma}}^{\mathbf{k}}$  are the Bogoliubov quasiparticle amplitudes on the  $\tilde{\mathbf{i}}$ -th site with corresponding momentum  $\mathbf{k}$  and eigenvalue  $E_n^{\mathbf{k}}$ . The SC pairing amplitude and electron densities are obtained through the following self-consistent equations,

$$\begin{aligned} \Delta &= \frac{V}{2} \sum_{\mathbf{k}, n} u_{n, \tilde{\mathbf{i}}, \sigma}^{\mathbf{k}} v_{n, \tilde{\mathbf{i}}, \bar{\sigma}}^{\mathbf{k}*} \tanh\left(\frac{E_n^{\mathbf{k}}}{2k_B T}\right) \\ n_{\tilde{\mathbf{i}}} &= \sum_{\mathbf{k}, n} \{|u_{n, \tilde{\mathbf{i}}, \uparrow}^{\mathbf{k}}|^2 f(E_n^{\mathbf{k}}) + |v_{n, \tilde{\mathbf{i}}, \downarrow}^{\mathbf{k}}|^2 [1 - f(E_n^{\mathbf{k}})]\}. \end{aligned} \quad (8)$$

Then, the single particle Green functions  $G_{\tilde{\mathbf{i}}\tilde{\mathbf{j}}}(\mathbf{k}, i\omega) = -\int_0^\beta d\tau \exp(i\omega\tau) \langle T_\tau c_{\tilde{\mathbf{k}}\tilde{\mathbf{i}}}^\dagger(i\tau) c_{\tilde{\mathbf{k}}\tilde{\mathbf{j}}}^\dagger(0) \rangle$  can be expressed as

$$G_{\tilde{\mathbf{i}}\tilde{\mathbf{j}}}(\mathbf{k}, i\omega) = \sum_n \left( \frac{u_{n, \tilde{\mathbf{i}}, \uparrow}^{\mathbf{k}} u_{n, \tilde{\mathbf{j}}, \uparrow}^{\mathbf{k}*}}{i\omega - E_n^{\mathbf{k}}} + \frac{v_{n, \tilde{\mathbf{i}}, \downarrow}^{\mathbf{k}} v_{n, \tilde{\mathbf{j}}, \downarrow}^{\mathbf{k}*}}{i\omega + E_n^{\mathbf{k}}} \right). \quad (9)$$

The spectral function  $A(\mathbf{k}, E)$  and the DOS  $\rho(E)$  can be derived respectively from the analytic continuation of the Green's function as,

$$A(\mathbf{k}, E) = -\frac{1}{N_P \pi} \sum_{\tilde{\mathbf{i}}} \text{Im} G_{\tilde{\mathbf{i}}\tilde{\mathbf{i}}}(\mathbf{k}, iE \rightarrow E + i0^+), \quad (10)$$

and

$$\rho(E) = \frac{1}{N_{\mathbf{k}}} \sum_{\mathbf{k}} A(\mathbf{k}, E), \quad (11)$$

where  $N_P$  and  $N_{\mathbf{k}}$  are the number of PUCs in the EUC and the number of  $\mathbf{k}$ -points in the Brillouin zone, respectively.

### III. RESULTS AND DISCUSSION

#### A. Spectral weight distribution and energy gap for the chiral flux phase

In this section, we investigate the low-energy spectral weight distribution and the energy gap in the chiral flux

phase. In the calculations, the chemical potential  $\mu$  is tuned so as to fix the band filling at  $1/6$  hole doping, i.e., the van Hove filling, which facilitates the inter-scatterings between three van Hove singularities with wave vectors  $\mathbf{Q}_{a,b,c}$ . The scatterings of the charge order, on the one hand, deplete the spectral weight on some portions of the FS, as shown in Fig. 1(c) for the low-energy ( $E = 0$ ) spectral weight distribution that is calculated directly in the PBZ. On the other hand, they fold the three bands in the PBZ of the PUC into the reduced Brillouin zone (RBZ) of the EUC, forming the twelve bands in the RBZ as presented in Fig. 1(d). Nevertheless, the results calculated straightly in the PBZ contain extra folded segments of spectral weight and energy bands [see Fig. 1(c), Fig. 3(b) and Fig. A1 for reference], and thus hinder the direct comparison to the original band structure or the experimental spectra in ARPES. Therefore, in the following, we will employ an unfolding procedure to recover the band structures and the spectral weights in the PBZ.

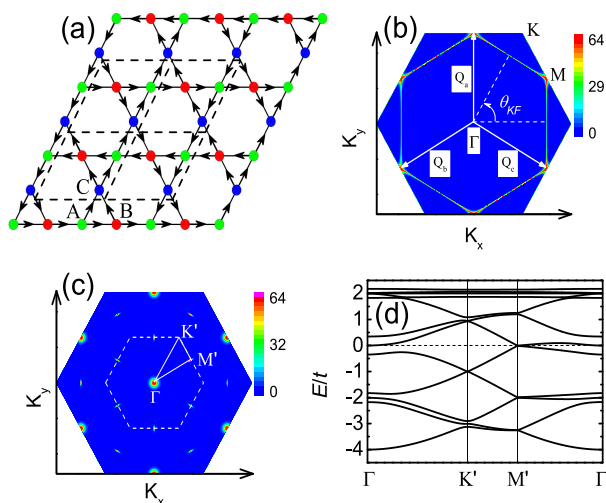


FIG. 1: (a) The lattice structure of the kagome superconductors, made out of three sublattices  $A$  (green dots),  $B$  (red dots) and  $C$  (blue dots). The arrows on the lattice depict the configuration of the orbital current, and the dashed lines denote the enlarged unit cell. (b) Fermi surface produced by the spectral weight distribution  $A^0(\mathbf{k}, E)$  at zero energy  $E = 0$ . (c) The spectral weight distribution  $A(\mathbf{k}, E)$  at zero energy  $E = 0$  obtained in the  $2 \times 2$  chiral flux phase with  $\lambda = 0.1$ . The hexagonal area in (c) surrounded by the white dashed lines shows the reduced Brillouin zone in the  $2 \times 2$  chiral flux phase. (d) The dispersion of the chiral flux phase along high-symmetry cuts in the reduced Brillouin zone for a typical value of  $\lambda = 0.1$ .

In Figs. 2(a) and (b), we show the unfolded spectral weight distribution  $A(\mathbf{k}, E)$  at  $E = 0$  in the chiral flux phase for  $\lambda = 0.02$  and  $\lambda = 0.1$ , respectively. In order to get a better view about the changes of the spectral weights for different  $\lambda$ , Fig. 2(c) also displays the unfolded spectral distribution along the momentum cut

from  $(\pi, -\sqrt{3}\pi/3)$  to  $(\pi, \sqrt{3}\pi/3)$  direction. As can be seen from the figures, the CDW scatterings not only depress the spectral weight and open the CDW gap on the FS, but also make the depression exhibit distinct momentum dependence. While the most depressed portion occurs near the  $M$  points for a weak  $\lambda$  and extends toward the midpoint of two adjacent  $M$  points with the increase of  $\lambda$ , a finite strength of spectral weight still remains around the midpoint and at the  $M$  points within the reasonable parameter regime  $\lambda \leq 0.5$ . Remarkably, the strength of spectral weight at the  $M$  points converges to a lower limit of one third of the intensity with the increase of  $\lambda$ , and accordingly a round spot, much like a van Hove singularity, with almost constant intensity of spectral weight appears at the  $M$  points.

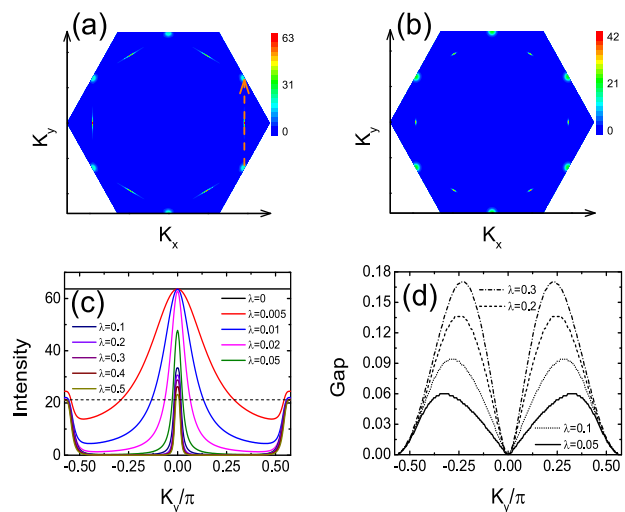


FIG. 2: The unfolded spectral weight distribution  $A(\mathbf{k}, E)$  at  $E = 0$  in the primitive Brillouin zone for  $\lambda = 0.02$  (a) and  $\lambda = 0.1$  (b), respectively. The dashed orange arrow in (a) indicates the momentum cut from  $(\pi, -\sqrt{3}\pi/3)$  to  $(\pi, \sqrt{3}\pi/3)$  direction. (c) The momentum distribution curves of the spectral weight along the momentum cut shown by the dashed orange arrow in (a) for different  $\lambda$ . The dashed line in (c) portrays one third of the intensity of  $\lambda = 0$ . (d) Evolution of the CDW gap along the momentum cut shown by the dashed orange arrow in (a) for different  $\lambda$ .

As a result of the momentum-dependent scatterings of the charge order, the CDW gap acquires the strong momentum dependence. Fig. 2(d) presents the CDW gaps for different  $\lambda$  along the momentum cut shown by the dashed orange arrow in Fig. 2(a), which are extracted from the spectral peak positions in the momentum-energy space. It is obvious that the CDW gap on the FS is anisotropic, with its zero minimum at the  $M$  points and at the midpoint of two adjacent  $M$  points, but exhibiting a maximum in the middle of these two zero minimums. We notice that the anisotropic CDW gap, including the positions of minimum and maximum, agrees

with the ARPES observations very well<sup>33</sup>.

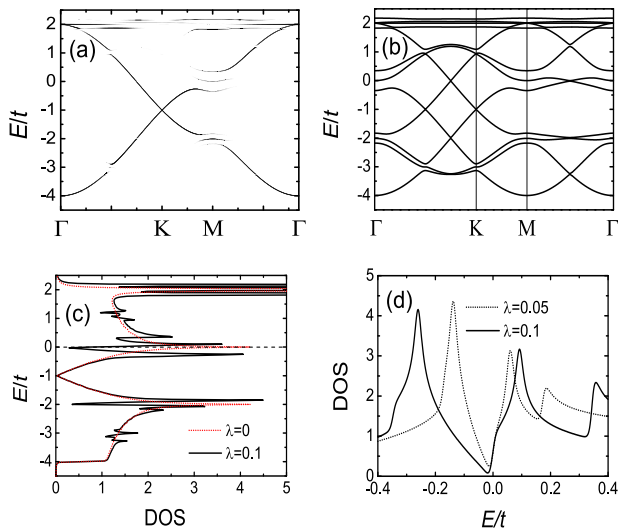


FIG. 3: (a) The unfolded dispersion of the chiral flux phase along high-symmetry cuts in the primitive Brillouin zone for a typical value of  $\lambda = 0.1$ . (b) The folded energy band dispersion of the chiral flux phase along high-symmetry cuts in the primitive Brillouin zone for a typical value of  $\lambda = 0.1$ . (c) Density of states in a wide energy range for the normal state (the red dotted curve) and the chiral flux state with  $\lambda = 0.1$  (the black solid curve). The dashed line is the Fermi level corresponding to the van Hove filling. (d) Density of states in the small energy scale for  $\lambda = 0.05$  and  $\lambda = 0.1$  in the chiral flux phase.

Considering the fact that the three scattering wave vectors connect the adjacent van Hove singular points ( $M$  points), the zero-energy van Hove singularity-like spot at the  $M$  points in the CDW state with the lower limit of intensity being exactly one third of that in the normal state is very intriguing and worth further clarification. It would be much more sensible to get insight from the physics of the three van Hove singular points at van Hove filling, where each of them comes exclusively from one of the three inequivalent lattice sites in the normal state<sup>38,65</sup> and are mutually coupled by the CDW order in the chiral flux phase. According to the configuration of the orbital current in Fig. 1(a), the low-energy effective theory at the  $M$  point for the CDW state is well described by the patch model<sup>55,57,66</sup>,

$$H_{CDW}(M) = \begin{pmatrix} \varepsilon_{M_A} & i\lambda & i\lambda \\ -i\lambda & \varepsilon_{M_B} & -i\lambda \\ -i\lambda & i\lambda & \varepsilon_{M_C} \end{pmatrix}, \quad (12)$$

where  $\varepsilon_{M_A}$  ( $\varepsilon_{M_B}$ ,  $\varepsilon_{M_C}$ ) stands for the energy at the van Hove singular point  $M_A$  ( $M_B$ ,  $M_C$ ) that originates from the sublattice  $A$  ( $B$ ,  $C$ ). At the van Hove filling with  $\varepsilon_{M_A} = \varepsilon_{M_B} = \varepsilon_{M_C} = 0$ , one can immediately find three eigenstates for the Hamiltonian  $H_{CDW}(M)$  with respective eigenvalues  $E_0(M) = 0$  and  $E_{\pm}(M) = \pm\sqrt{3}\lambda$ , and

each of these three eigenstates weights one third of the total probability. This is to say the zero-energy state at van Hove singular point  $M$  triply splits into three energy states with each of them possessing one third of the total spectral weights.

Interestingly, the very simple argument is indeed embodied in the momentum distribution curves of the unfolded spectral weight and the unfolded energy dispersion in momentum space along high-symmetry cuts shown respectively in Figs. 2(c) and 3(a). As illustrated in these figures, the original band near the upper saddle point is triply split by the charge order scatterings to the upper, middle and lower branches, where the middle one characterizes a new saddle-shaped band just at the Fermi energy with its spectral weight approaching one third of that in the normal state. By contrast, the Dirac point around the  $K$  point remains nearly intact upon entering the chiral flux phase. For comparison, we also present the folded energy band dispersion of the chiral flux phase along the high-symmetry cuts in the PBZ in Fig. 3(b). More detailed energy band changes with  $\lambda$  can be found in Appendix A. As a result, the effect of a weak chiral flux charge order on the DOS mainly concentrates on the near-by energies of the van Hove singularity, as can be seen by making a comparison between the black solid and the red dotted curves in Fig. 3(c) and in Fig. 3(d) for the enlarged view of the low energy DOS. This implies the orbital current order would have a profound impact on the SC properties, which have been proposed to derive benefit from the van Hove singularities.

Thus far, we have demonstrated that the proposed chiral flux CDW phase for the kagome superconductors exhibits some typical features, including the momentum-dependent partial gap opening at Fermi energy, the emergence of the new saddle point at the  $M$  point and the unchanged Dirac point as well, which are all in good accordance with the experimental observations<sup>22,33,67</sup>. It is worth pointing out that the unique change of the spectral function from the normal state to the CDW state can be used as an indirect evidence to identify the time-reversal symmetry-breaking CDW state. For the CDW state with time-reversal symmetry, the off-diagonal elements in Eq. (12) are real, which leads to the band at  $M$  point splitting into only two sub-bands with unequal spectral weights.

## B. Modulated $s$ -wave SC pairing and nodal gap

Having analyzed the spectral and gap features of the chiral flux CDW phase, we now pursue the main question of the paper, i.e., the impact of the chiral flux order on the SC properties. In the calculations, the SC order parameter is determined self-consistently by treating the orbital current order  $\lambda$  as a variable argument. In Figs. 4(a)-(e), we present the intensity plots of the spectral function in the coexistence of orbital current and SC orders as functions of energy and momentum along the

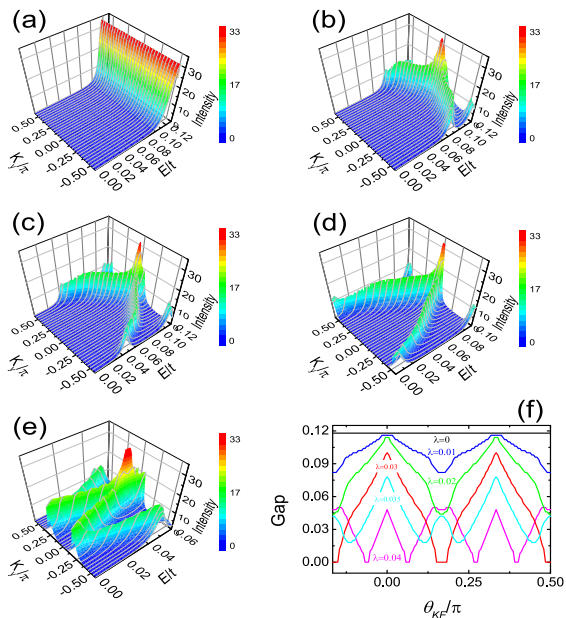


FIG. 4: The intensity plots of the unfolded spectral function as functions of the momentum and energy in the coexistent state for different strength of  $\lambda = 0$  (a),  $\lambda = 0.01$  (b),  $\lambda = 0.02$  (c),  $\lambda = 0.03$  (d), and  $\lambda = 0.04$  (e), respectively. The momentum in each panel is along the cut from  $(\pi, -\sqrt{3}\pi/3)$  to  $(\pi, \sqrt{3}\pi/3)$  direction, as denoted by the dashed orange arrow in Fig. 2(a). (f) Evolution of the gap along the Fermi surface as a function of  $\theta_{k_F}$  for different strength of  $\lambda$ . The gap is extracted from the peak positions of the spectral function in panels (a)-(e).

cut shown as the dashed orange arrow in Fig. 2(a). For  $\lambda = 0$  in Fig. 4(a), the intensity of the spectral function shows a gap edge structure at constant energy, from which an isotropic gap feature indicated by the black solid line in Fig. 4(f) can be extracted on the FS as a function of  $\theta_{k_F}$ , with the angle of the Fermi momentum  $\theta_{k_F}$  being defined in Fig. 1(b). Correspondingly, one can see a typical U-shaped full gap structure for the DOS in Figs. 5(a)-(e), where the DOS for  $\lambda = 0$  is plotted with the black curve in all panels for reference.

Inclusion of a small value of  $\lambda$ , say for example  $\lambda < 0.02$ , has little bearing on the SC pairing amplitude  $\Delta$  [see Fig. 5(f)], but has an obvious effect on the the spectral function distribution and the line shape of DOS. Specifically, the introduction of a tiny value of the orbital current order, such as  $\lambda = 0.01$ , will cause the red-shift of the gap edge. As the CDW order partially gaps the FS with the utmost strength of the scattering occurring at the  $M$  points, the SC softening is expected to start from the  $M$  points. This is evidenced by the drawing in Fig. 4(b), where the shift is clearly visible to begin at the  $M$  points, and reach its minimum at the midpoint of the momentum cut, leading to the modulation of the gap on the FS, as displayed by the blue curve in Fig. 4(f). As a result, the DOS changes its U-shaped curve to a

basin-like one along with the slightly blunted gap edges, as depicted by the red curve in Fig. 5(a).

Whereas the position of the gap edge at the midpoint of the momentum cut shifts slightly toward lower energies with the increase of  $\lambda$ , it decreases significantly at the  $M$  points, as illustrated in Figs. 4(b)-(c). As is seen in Fig. 4(f), the striking contrast of the gap edge shifts between the  $M$  points and the midpoint results in the deeper modulation depth of the spectral gap on the FS with a stronger orbital current order. Consequently, one can expect the appearance of the gap nodes on the FS when the orbital current order reaches a certain level such as  $\lambda \sim 0.03$ . Further increase in the orbital current order will remove the gap nodes by lifting the quasiparticle energies around the  $M$  points on one hand, and on the other hand it pushes the energies downward on the portion between the  $M$  point and the midpoint [see Fig. 4(f) for  $\lambda = 0.035$ ]. As a result, the period of the gap modulation on the FS becomes shorter than that of the smaller  $\lambda$ , and leads to the doubling of the nodal portions on the FS as the orbital current order achieving to about  $\lambda = 0.04$ , as is shown in Fig. 4(f). It is noteworthy that the results with sign preserved nodal gap we identified here come to the same conclusion with the experiment<sup>13</sup>.

With the increase of  $\lambda$ , the line shape of the DOS follows the corresponding changes with the spectral weight function. On one hand, accompanied by the decrease of the SC pairing amplitude  $\Delta$  [see Fig. 5(f)], the basin-like DOS is continually deformed to a V-shaped one by the increase of  $\lambda$ , as evidenced in Figs. 5(b)-(d). On the other hand, the appearance of multiple sets of gap edge peak can be clearly seen in Figs. 5(b)-(d) for  $\lambda \geq 0.02$ . Moreover, as  $\lambda$  is increased, there exists residual DOS at zero energy in Figs. 5(c) and (d). The V-shaped DOS with multiple sets of gap edge peak and residual zero-energy DOS constitutes a characteristic of a nodal multi-gap SC pairing state. Although a single orbital tight-binding model and the conventional on-site  $s$ -wave SC pairing are adopted here, it is very interesting that the salient features such as the V-shaped DOS, the residual zero-energy DOS as well as the multiple sets of gap edge peak produced in the coexistence of orbital current order and SC pairing are in good accordance with the STM experiments<sup>12-14</sup>.

As the orbital current order increases to  $\lambda \sim 0.05$ , the system is driven to the phase of dominant CDW order by heavily suppressing the SC pairing amplitude [see Fig. 5(f)]. Accordingly, the DOS for  $\lambda = 0.05$  presented in Fig. 5(e) turns to the result in Fig. 3(d) for the pure chiral flux phase. The result suggests that the strength of the orbital current order needs to be treated with caution when one studies the interplay between the SC and orbital current order in a non-self-consistent manner<sup>61</sup>, because the superconductivity would be totally suppressed by even the moderate orbital current order.

Clarification of the interplay between the time-reversal symmetry-breaking charge orders and superconductivity is a key step toward the understanding of the underly-

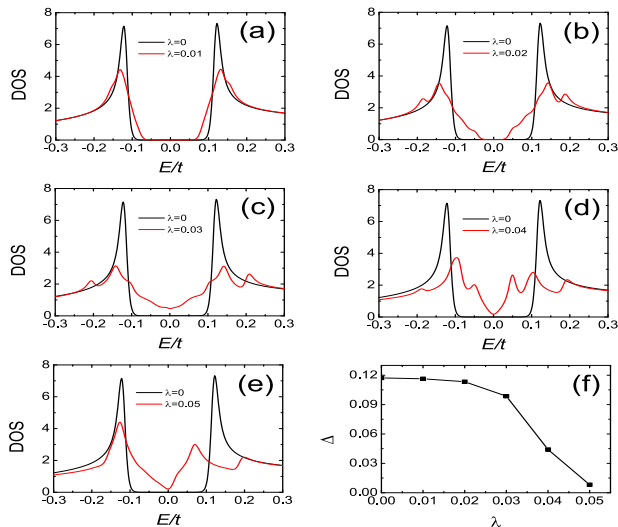


FIG. 5: (a)-(e) The energy dependence of the DOS for different strength of  $\lambda$ . (f) Evolution of the SC pairing  $\Delta$  as a function of  $\lambda$ .

ing physics of the V-based kagome superconductors. Although the competition nature between them has been identified in these materials, there is accumulating evidence that also shows a coexistence of them. It has been observed that the CDW in  $AV_3Sb_5$  intertwined with SC order could result in the spatial modulations of the SC gap, i.e., the so called roton pair-density wave state<sup>12</sup>. In this paper, we have demonstrated that the orbital current order can lead to the gap modulations on the FS. While the spatial modulations of the gap have been probed by means of STM/STS measurement, the gap modulations on the FS can be discernable in the ARPES and field angle-dependent thermal conductivity measurements for identifying the interplay between the CDW and the SC orders, and for verifying or falsifying the above scenario. Whether there is a relationship between the gap modulations on the FS in the present study and the experimental observations of the roton pair-density wave, or if there is a possibility that the orbital current order could also lead to some spatial modulations of the SC pairing, constitute the fascinating questions deserving further studies.

#### IV. CONCLUSION

In conclusion, we have studied the impact of the chiral flux CDW order on the experimental outcomes for the normal and the SC properties. With the aids of the unfolding procedure to the PBZ, it was revealed that a new

saddle point turns up at  $M$  points near the Fermi energy to form the van Hove singularity-like spectral spots in the CDW phase, despite that the original band near the Fermi energy could be gaped by the CDW order. The band gap was manifested in the partially gaped spectral weight on the FS with the reservation of the spectral weight on the  $M$  points and the midpoint between the two adjacent  $M$  points. In the environment of the partially gaped FS and the new van Hove singularity-like spot, a conventional fully gapped SC pairing would have a chance to survive in the coexistence of the chiral flux CDW and SC orders, at the expense of the spectral gap modulations on the FS. Owing to the modulations of the gap, a nodal gap feature for the spectral weight might appear on the FS under certain strengths of the CDW order. Accordingly, the U-shaped DOS deformed to the V-shaped one along with the residual DOS near the Fermi energy. These results were concordant with the experimental observations in many aspects, and might serve as a proposal to mediate the divergent or seemingly contradictory experimental outcomes with respect to the SC pairing symmetry.

#### V. ACKNOWLEDGEMENT

This work was supported by the National Natural Science Foundation of China (Grant No. 12074175).

#### Appendix A: Folded and unfolded band structures for different $\lambda$

In Fig. A1, we present the folded band structures and the unfolded dispersion of the spectral weight along high-symmetry cuts in the PBZ for the chiral flux phase with different  $\lambda$ . First of all, the triple splitting of the energy band near the van Hove points happens for all cases with the splitting being proportional to the charge order strength  $\lambda$  (Note that the triple splitting is obviously weakened at the lower van Hove point due to the non-zero energy of this point and the mixing contributions from different sublattices.). Secondly, the low energy portion along the  $\Gamma$  to  $K$  direction remains intact when the CDW order is not too strong such as  $\lambda \leq 0.1$ , but it is gapped by the strong CDW order with  $\lambda = 0.2$  and  $\lambda = 0.3$  with the upper branch just touching the Fermi level, which clearly manifest in Figs. A1(b), (d), (f) and (h) for the unfolded spectral dispersion. Besides, the Dirac bands near the  $K$  point always maintain the same basic feature for the parameters considered here.

\* Electronic address: monsoonjhm@sina.com

† Electronic address: slyu@nju.edu.cn

<sup>1</sup> B. R. Ortiz, S. M. L. Teicher, Y. Hu, J. L. Zuo, P. M. Sarte, E. C. Schueller, A. M. M. Abeykoon, M. J. Krogstad, S.

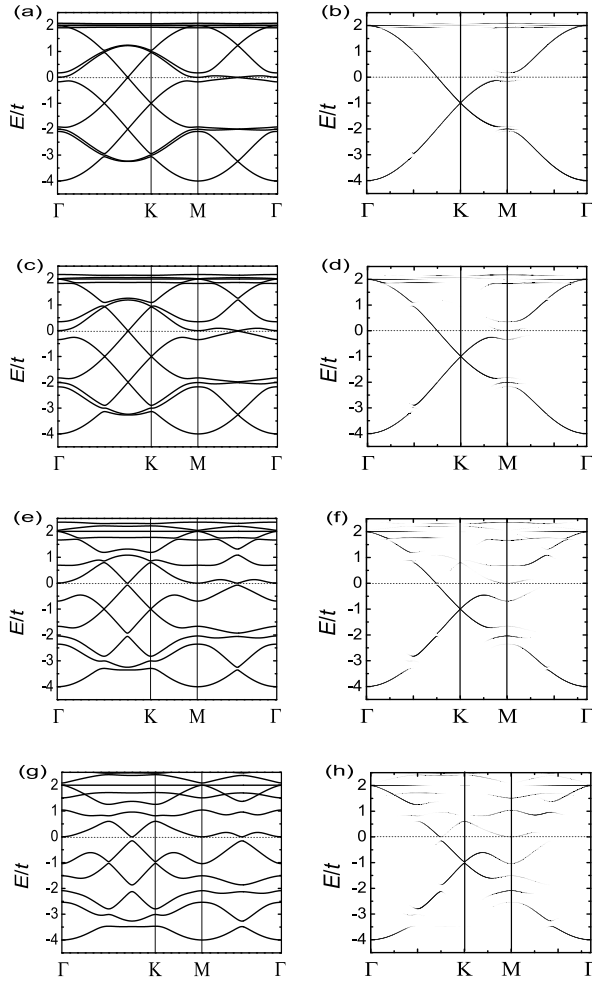


FIG. A1: The folded (left column) and unfolded (right column) band structures of the chiral flux charge order phase along high-symmetry cuts in the primitive Brillouin zone for  $\lambda = 0.05$  [(a), (b)],  $\lambda = 0.1$  [(c), (d)],  $\lambda = 0.2$  [(e), (f)] and  $\lambda = 0.3$  [(g), (h)] respectively.

Rosenkranz, R. Osborn, R. Seshadri, L. Balents, J. He, and S. D. Wilson, *Phys. Rev. Lett.* **125**, 247002 (2020).

<sup>2</sup> S.-Y. Yang, Y. Wang, B. R. Ortiz, D. Liu, J. Gayles, E. Derunova, R. Gonzalez-Hernandez, L. Šmejkal, Y. Chen, S. S. P. Parkin, S. D. Wilson, E. S. Toberer, T. McQueen, and M. N. Ali, *Sci. Adv.* **6**, eabb6003 (2020).

<sup>3</sup> B. R. Ortiz, P. M. Sarte, E. M. Kenney, M. J. Graf, S. M. L. Teicher, R. Seshadri, and S. D. Wilson, *Phys. Rev. Mater.* **5**, 034801 (2021).

<sup>4</sup> Q. Yin, Z. Tu, C. Gong, Y. Fu, S. Yan, and H. Lei, *Chin. Phys. Lett.* **38**, 037403 (2021).

<sup>5</sup> K. Y. Chen, N. N. Wang, Q. W. Yin, Y. H. Gu, K. Jiang, Z. J. Tu, C. S. Gong, Y. Uwatoko, J. P. Sun, H. C. Lei, J. P. Hu, and J.-G. Cheng, *Phys. Rev. Lett.* **126**, 247001 (2021).

<sup>6</sup> Y. Wang, S. Yang, P. K. Sivakumar, B. R. Ortiz, S. M. L. Teicher, H. Wu, A. K. Srivastava, C. Garg, D. Liu, S. S. P. Parkin, E. S. Toberer, T. McQueen, S. D. Wilson, and M. N. Ali, arXiv:2012.05898.

<sup>7</sup> Z. Zhang, Z. Chen, Y. Zhou, Y. Yuan, S. Wang, J. Wang,

H. Yang, C. An, L. Zhang, X. Zhu, Y. Zhou, X. Chen, J. Zhou, and Z. Yang, *Phys. Rev. B* **103**, 224513 (2021).

<sup>8</sup> Y.-X. Jiang, J.-X. Yin, M. M. Denner, N. Shumiya, B. R. Ortiz, G. Xu, Z. Guguchia, J. He, M. S. Hossain, X. Liu, J. Ruff, L. Kautzsch, S. S. Zhang, G. Chang, I. Belopolski, Q. Zhang, T. A. Cochran, D. Multer, M. Litskevich, Z.-J. Cheng, X. P. Yang, Z. Wang, R. Thomale, T. Neupert, S. D. Wilson, and M. Z. Hasan, *Nat. Mater.* **20**, 1353 (2021).

<sup>9</sup> F. H. Yu, T. Wu, Z. Y. Wang, B. Lei, W. Z. Zhuo, J. J. Ying, and X. H. Chen, *Phys. Rev. B* **104**, L041103 (2021).

<sup>10</sup> X. Chen, X. Zhan, X. Wang, J. Deng, X.-B. Liu, X. Chen, J.-G. Guo, and X. Chen, *Chin. Phys. Lett.* **38**, 057402 (2021).

<sup>11</sup> H. Zhao, H. Li, B. R. Ortiz, S. M. L. Teicher, T. Park, M. Ye, Z. Wang, L. Balents, S. D. Wilson, and I. Zeljkovic, *Nature* **599**, 216 (2021).

<sup>12</sup> H. Chen, H. Yang, B. Hu, Z. Zhao, J. Yuan, Y. Xing, G. Qian, Z. Huang, G. Li, Y. Ye, S. Ma, S. Ni, H. Zhang, Q. Yin, C. Gong, Z. Tu, H. Lei, H. Tan, S. Zhou, C. Shen, X. Dong, B. Yan, Z. Wang, and H.-J. Gao, *Nature* **599**, 222 (2021).

<sup>13</sup> H.-S. Xu, Y.-J. Yan, R. Yin, W. Xia, S. Fang, Z. Chen, Y. Li, W. Yang, Y. Guo, and D.-L. Feng, *Phys. Rev. Lett.* **127**, 187004 (2021).

<sup>14</sup> Z. Liang, X. Hou, F. Zhang, W. Ma, P. Wu, Z. Zhang, F. Yu, J.-J. Ying, K. Jiang, L. Shan, Z. Wang, and X.-H. Chen, *Phys. Rev. X* **11**, 031026 (2021).

<sup>15</sup> C. Mu, Q. Yin, Z. Tu, C. Gong, H. Lei, Z. Li, and J. Luo, *Chin. Phys. Lett.* **38**, 077402 (2021).

<sup>16</sup> W. Duan, Z. Nie, S. Luo, F. Yu, B. R. Ortiz, L. Yin, H. Su, F. Du, A. Wang, Y. Chen, X. Lu, J. Ying, S. D. Wilson, X. Chen, Y. Song, and H. Yuan, *Sci. China-Phys. Mech. Astron.* **64**, 107462 (2021).

<sup>17</sup> C. C. Zhao, L. S. Wang, W. Xia, Q. W. Yin, J. M. Ni, Y. Y. Huang, C. P. Tu, Z. C. Tao, Z. J. Tu, C. S. Gong, H. C. Lei, Y. F. Guo, X. F. Yang, and S. Y. Li, arXiv: 2102.08356.

<sup>18</sup> S. Ni, S. Ma, Y. Zhang, J. Yuan, H. Yang, Z. Lu, N. Wang, J. Sun, Z. Zhao, D. Li, S. Liu, H. Zhang, H. Chen, K. Jin, J. Cheng, L. Yu, F. Zhou, X. Dong, J. Hu, H.-J. Gao, and Z. Zhao, *Chin. Phys. Lett.* **38**, 057403 (2021).

<sup>19</sup> Y. Xiang, Q. Li, Y. Li, W. Xie, H. Yang, Z. Wang, Y. Yao, and H.-H. Wen, *Nat. Commun.* **12**, 6727 (2021).

<sup>20</sup> B. R. Ortiz, S. M. L. Teicher, L. Kautzsch, P. M. Sarte, N. Ratcliff, J. Harter, J. P. C. Ruff, R. Seshadri, and S. D. Wilson, *Phys. Rev. X* **11**, 041030 (2021).

<sup>21</sup> X. Zhou, Y. Li, X. Fan, J. Hao, Y. Dai, Z. Wang, Y. Yao, and H.-H. Wen, *Phys. Rev. B* **104**, L041101 (2021).

<sup>22</sup> Z. Liu, N. Zhao, Q. Yin, C. Gong, Z. Tu, M. Li, W. Song, Z. Liu, D. Shen, Y. Huang, K. Liu, H. Lei, and S. Wang, *Phys. Rev. X* **11**, 041010 (2021).

<sup>23</sup> M. Kang, S. Fang, J.-K. Kim, B. R. Ortiz, S. H. Ryu, J. Kim, J. Yoo, G. Sangiovanni, D. D. Sante, B.-G. Park, C. Jozwiak, A. Bostwick, E. Rotenberg, E. Kaxiras, S. D. Wilson, J.-H. Park, and R. Comin, *Nat. Phys.* **18**, 301 (2022).

<sup>24</sup> Y. Fu, N. Zhao, Z. Chen, Q. Yin, Z. Tu, C. Gong, C. Xi, X. Zhu, Y. Sun, K. Liu, and H. Lei, *Phys. Rev. Lett.* **127**, 207002 (2021).

<sup>25</sup> Y. Song, T. Ying, X. Chen, X. Han, X. Wu, A. P. Schnyder, Y. Huang, J.-g. Guo, and X. Chen, *Phys. Rev. Lett.* **127**, 237001 (2021).

<sup>26</sup> H. Tan, Y. Liu, Z. Wang, and B. Yan, *Phys. Rev. Lett.* **127**, 046401 (2021).



- <sup>27</sup> N. Shumiya, Md. S. Hossain, J.-X. Yin, Y.-X. Jiang, B. R. Ortiz, H. Liu, Y. Shi, Q. Yin, H. Lei, S. S. Zhang, G. Chang, Q. Zhang, T. A. Cochran, D. Multer, M. Litskevich, Z.-J. Cheng, X. P. Yang, Z. Guguchia, S. D. Wilson, and M. Z. Hasan, *Phys. Rev. B* **104**, 035131 (2021).
- <sup>28</sup> F. H. Yu, D. H. Ma, W. Z. Zhuo, S. Q. Liu, X. K. Wen, B. Lei, J. J. Ying, and X. H. Chen, *Nat. Commun.* **12**, 3645 (2021).
- <sup>29</sup> L. Yin, D. Zhang, C. Chen, G. Ye, F. Yu, B. R. Ortiz, S. Luo, W. Duan, H. Su, J. Ying, S. D. Wilson, X. Chen, H. Yuan, Y. Song, and X. Lu, *Phys. Rev. B* **104**, 174507 (2021).
- <sup>30</sup> K. Nakayama, Y. Li, T. Kato, M. Liu, Z. Wang, T. Takahashi, Y. Yao, and T. Sato, *Phys. Rev. B* **104**, L161112 (2021).
- <sup>31</sup> K. Jiang, T. Wu, J.-X. Yin, Z. Wang, M. Z. Hasan, S. D. Wilson, X. Chen, and J. Hu, arXiv: 2109.10809.
- <sup>32</sup> L. Nie, K. Sun, W. Ma, D. Song, L. Zheng, Z. Liang, P. Wu, F. Yu, J. Li, M. Shan, D. Zhao, S. Li, B. Kang, Z. Wu, Y. Zhou, K. Liu, Z. Xiang, J. Ying, Z. Wang, T. Wu, and X. Chen, *Nature* **604**, 59 (2022).
- <sup>33</sup> H. Luo, Q. Gao, H. Liu, Y. Gu, D. Wu, C. Yi, J. Jia, S. Wu, X. Luo, Y. Xu, L. Zhao, Q. Wang, H. Mao, G. Liu, Z. Zhu, Y. Shi, K. Jiang, J. Hu, Z. Xu, and X. J. Zhou, *Nat. Commun.* **13**, 273 (2022).
- <sup>34</sup> T. Neupert, M. M. Denner, J.-X. Yin, R. Thomale, and M. Z. Hasan, *Nat. Phys.* **18**, 137 (2022).
- <sup>35</sup> K. Nakayama, Y. Li, T. Kato, M. Liu, Z. Wang, T. Takahashi, Y. Yao, and T. Sato, *Phys. Rev. X* **12**, 011001 (2022).
- <sup>36</sup> H. Li, S. Wan, H. Li, Q. Li, Q. Gu, H. Yang, Y. Li, Z. Wang, Y. Yao, and H.-H. Wen, *Phys. Rev. B* **105**, 045102 (2022).
- <sup>37</sup> C. Guo, C. Putzke, S. Konyzheva, X. Huang, M. Gutierrez-Amigo, I. Errea, D. Chen, M. G. Vergniory, C. Felser, M. H. Fischer, T. Neupert, and P. J. W. Moll, *Nature* **611**, 461 (2022).
- <sup>38</sup> S.-L. Yu and J.-X. Li, *Phys. Rev. B* **85**, 144402 (2012).
- <sup>39</sup> M. L. Kiesel and R. Thomale, *Phys. Rev. B* **86**, 121105(R) (2012).
- <sup>40</sup> W.-S. Wang, Z.-Z. Li, Y.-Y. Xiang, and Q.-H. Wang, *Phys. Rev. B* **87**, 115135 (2013).
- <sup>41</sup> M. L. Kiesel, C. Platt, and R. Thomale, *Phys. Rev. Lett.* **110**, 126405 (2013).
- <sup>42</sup> X. Wu, T. Schwemmer, T. Müller, A. Consiglio, G. Sangiovanni, D. Di Sante, Y. Iqbal, W. Hanke, A. P. Schnyder, M. M. Denner, M. H. Fischer, T. Neupert, and R. Thomale, *Phys. Rev. Lett.* **127**, 177001 (2021).
- <sup>43</sup> C. Wen, X. Zhu, Z. Xiao, N. Hao, R. Mondaini, H.-M. Guo, and S. Feng, *Phys. Rev. B* **105**, 075118 (2022).
- <sup>44</sup> R. Tazai, Y. Yamakawa, S. Onari, and H. Kontani, *Sci. Adv.* **8**, eabl4108 (2022).
- <sup>45</sup> B. R. Ortiz, L. C. Gomes, J. R. Morey, M. Winiarski, M. Bordelon, J. S. Mangum, I. W. H. Oswald, J. A. Rodriguez-Rivera, J. R. Neilson, S. D. Wilson, E. Ertekin, T. M. McQueen, and E. S. Toberer, *Phys. Rev. Mater.* **3**, 094407 (2019).
- <sup>46</sup> E. M. Kenney, B. R. Ortiz, C. Wang, S. D. Wilson, and M. J. Graf, *J. Phys.: Condens. Matter* **33**, 235801 (2021).
- <sup>47</sup> C. Mielke III, D. Das, J.-X. Yin, H. Liu, R. Gupta, Y.-X. Jiang, M. Medarde, X. Wu, H. C. Lei, J. Chang, P. Dai, Q. Si, H. Miao, R. Thomale, T. Neupert, Y. Shi, R. Khasanov, M. Z. Hasan, H. Luetkens, and Z. Guguchia, *Nature* **602**, 245 (2022).
- <sup>48</sup> L. Yu, C. Wang, Y. Zhang, M. Sander, S. Ni, Z. Lu, S. Ma, Z. Wang, Z. Zhao, H. Chen, K. Jiang, Y. Zhang, H. Yang, F. Zhou, X. Dong, S. L. Johnson, M. J. Graf, J. Hu, H.-J. Gao, and Z. Zhao, arXiv:2107.10714.
- <sup>49</sup> Y. Xu, Z. Ni, Y. Liu, B. R. Ortiz, Q. Deng, S. D. Wilson, B. Yan, L. Balents, and L. Wu, *Nat. Phys.* **18**, 1470 (2022).
- <sup>50</sup> X. Zhou, H. Liu, W. Wu, K. Jiang, Y. Shi, Z. Li, Y. Sui, J. Hu, and J. Luo, *Phys. Rev. B* **105**, 205104 (2022).
- <sup>51</sup> D. Chen, B. He, M. Yao, Y. Pan, H. Lin, W. Schnelle, Y. Sun, J. Gooth, L. Taillefer, and C. Felser, *Phys. Rev. B* **105**, L201109 (2022).
- <sup>52</sup> Q. Wu, Z. X. Wang, Q. M. Liu, R. S. Li, S. X. Xu, Q. W. Yin, C. S. Gong, Z. J. Tu, H. C. Lei, T. Dong, and N. L. Wang, *Phys. Rev. B* **106**, 205109 (2022).
- <sup>53</sup> Y. Hu, S. Yamane, G. Mattoni, K. Yada, K. Obata, Y. Li, Y. Yao, Z. Wang, J. Wang, C. Farhang, J. Xia, Y. Maeno, and S. Yonezawa, arXiv:2208.08036.
- <sup>54</sup> J. W. F. Venderbos, *Phys. Rev. B* **93**, 115107 (2016).
- <sup>55</sup> Y.-P. Lin and R. M. Nandkishore, *Phys. Rev. B* **100**, 085136 (2019).
- <sup>56</sup> T. Park, M. Ye, and L. Balents, *Phys. Rev. B* **104**, 035142 (2021).
- <sup>57</sup> Y.-P. Lin and R. M. Nandkishore, *Phys. Rev. B* **104**, 045122 (2021).
- <sup>58</sup> X. Feng, K. Jiang, Z. Wang, and J. Hu, *Sci. Bull.* **66**, 1384 (2021).
- <sup>59</sup> X. Feng, Y. Zhang, K. Jiang, and J. Hu, *Phys. Rev. B* **104**, 165136 (2021).
- <sup>60</sup> M. M. Denner, R. Thomale, and T. Neupert, *Phys. Rev. Lett.* **127**, 217601 (2021).
- <sup>61</sup> Y. Gu, Y. Zhang, X. Feng, K. Jiang, and J. Hu, *Phys. Rev. B* **105**, L100502 (2022).
- <sup>62</sup> Y.-P. Lin and R. M. Nandkishore, *Phys. Rev. B* **106**, L060507 (2022).
- <sup>63</sup> J.-W. Dong, Z. Wang, and S. Zhou, arXiv:2209.10768.
- <sup>64</sup> L. Zheng, Z. Wu, Y. Yang, L. Nie, M. Shan, K. Sun, D. Song, F. Yu, J. Li, D. Zhao, S. Li, B. Kang, Y. Zhou, K. Liu, Z. Xiang, J. Ying, Z. Wang, T. Wu, and X. Chen, *Nature* **611**, 682 (2022).
- <sup>65</sup> H.-M. Jiang, S.-L. Yu, and X.-Y. Pan, *Phys. Rev. B* **106**, 014501 (2022).
- <sup>66</sup> R. Nandkishore, L. S. Levitov, and A. V. Chubukov, *Nat. Phys.* **8**, 158 (2012).
- <sup>67</sup> S. Cho, H. Ma, W. Xia, Y. Yang, Z. Liu, Z. Huang, Z. Jiang, X. Lu, J. Liu, Z. Liu, J. Li, J. Wang, Y. Liu, J. Jia, Y. Guo, J. Liu, and D. Shen, *Phys. Rev. Lett.* **127**, 236401 (2021).